

Anisotropic deformation of Rydberg blockade sphere in few-atom systems

Jing Qian,¹Xing-Dong Zhao,²Lu Zhou¹ and Weiping Zhang¹

¹*Quantum Institute for Light and Atoms, Department of Physics,
East China Normal University, Shanghai 200062, China and*

²*Department of Physics, Henan Normal University, Xinxiang 453007, China*

Rydberg blockade sphere persists an intriguing picture by which a number of collective many-body effects caused by the strong Rydberg-Rydberg interactions can be clearly understood and profoundly investigated. In the present work, we develop a new definition for the effective two-atom blockade radius and show that the original spherically shaped blockade surface would be deformed when the real number of atoms increases from two to three. This deformation of blockade sphere reveals spatially anisotropic and shrunken properties which strongly depend on the interatomic distance. In addition, we also study the optimal conditions for the Rydberg antiblockade effect and make predictions for improving the antiblockade efficiency in few-atom systems.

PACS numbers:

I. INTRODUCTION

Blockade sphere can provide an intuitive picture to understand a number of quantum many-body phenomena in strongly interacting Rydberg systems [1], for example, the critical behavior for quantum phase transition [2], dynamical crystallization [3], Rydberg solitons [4] and so on. Within a blockade sphere, the multi-atom excitations are significantly suppressed owing to the large energy shift induced by the strong Rydberg-Rydberg interactions (RRIs), leading to a collective enhancement for the single-atom transition dipole by a factor of \sqrt{N} (N is the atomic number in the sphere). In a mesoscopic atomic ensemble with $N \gg 1$, the collective Rabi frequency is enhanced to $\sqrt{N}\Omega$ and it acts as a "superatom" [5]. With this idea, a saturable single photon absorber is designed for the manipulation of photon-matter interactions [6]. The underlying physics behind *blockade sphere* is *Rydberg blockade mechanism*, which was first proposed to control quantum logic gate and generate nonclassical photonic states [7, 8]. In recent years many experimental achievements prove the observation of single-atom collective excitation induced by the RRIs in ultracold mesoscopic ensembles [9–11] as well as in two atoms [12, 13]. A significant reduction of the blockade size due to the Doppler effect is observed in room temperature atomic samples [14] and can be overcome with a pulsed four-wave mixing scheme [15]. These observations hold promises for further studies in quantum information science by using strongly interacting Rydberg atoms [16, 17].

To characterize such a *sphere*, defining a good blockade radius is a key ingredient by which we can classify the whole blockade regimes into strong blockade, partial blockade and non-blockade regimes according to the relative strengths between the RRI energy and the linewidth of excitation. So far, a large number of experiments and theoretical works are performed in the strong blockade regime [18–21] where a perfect blocked phenomenon for the doubly excited state population is identified [22, 23] and the formation of plasmas due to an ionization avalanche is observed [24]. More recently,

L. Béguin *et al.* report a direct measurement of the van der Waals (vdWs) interaction between two Rydberg atoms in the partial blockade regime in which the population oscillations exhibit several vdWs energy-dependent frequencies rather than single collective Rabi frequency [25]. In order to investigate quantum dynamics in such strong blockade and partial blockade regimes, one always adopts a spherical-shaped model with its volume $(4/3)\pi r_b^3$ and radius r_b (typically a few microns) defined as the interatomic distance at which the vdWs interaction equals the excitation linewidth of single atom [26–28]. This spherical shape assumption is robust under the condition of mean two-atom distance being significantly smaller than r_b in a superatom, i.e. the case of strong blockade; however, if they two become comparable in the partial blockade regime, we predict that the spherical surface would become deformed, leading to an inefficient Rydberg blockade.

In a recent work, T. Pohl and P. Berman show that the two-atom Rydberg blockade will break down when the number of atoms increases from two to three [29]. Here, we propose an alternative opinion to extend this model by introducing the blockade sphere picture. The purpose of this work is to investigate the spatially anisotropic deformations of Rydberg blockade sphere in a three-atom system where the deformation strength is well determined by the two-atom distance. For non-interacting or strongly interacting atoms, the two-atom blockade sphere picture is a feasible tool to characterize and even optimize the blockade efficiency for multi-atom ensembles. However, for partial blockade, the coherent atomic excitations behave much complex, which makes the simple two-atom blockade sphere model ineffective. In addition to the complete analytical results of a two-atom system, we numerically solve the master equations for three atoms and represent various deformed surfaces in a two-dimensional (2D) space. Besides, we develop an optimal antiblockade condition in few-atom systems, which is also useful for multiple atom ensembles.

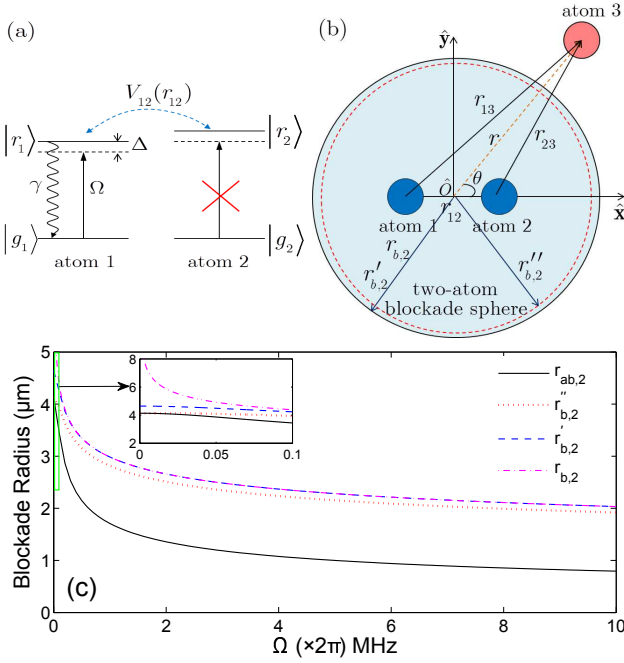


FIG. 1: (Color online) (a) Schematic representation of two-atom Rydberg blockade. Each atom has a ground state $|g_{1(2)}\rangle$ and a Rydberg state $|r_{1(2)}\rangle$ which are illuminated by a cw laser field with Rabi frequency Ω and one-photon detuning Δ . γ describes the corresponding spontaneous decay process from the excited state to the ground state. Due to the energy shift of state $|r_1 r_2\rangle$ caused by the Rydberg-Rydberg state interaction $V_{12}(r_{12})$, the laser is out of resonance for the transition from singly symmetric excited state $(|g_1 r_2\rangle + |r_1 g_2\rangle)/\sqrt{2}$ to doubly excited state $|r_1 r_2\rangle$, and only one atom (e.g. atom 1) can be excited to $|r_1\rangle$. (b) Two atoms 1 and 2 are prepared with separation r_{12} in a 2D space, creating a blockade sphere. A third atom is placed in the same space, with the separations r_{13} and r_{23} from atoms 1 and 2, respectively. Its position is denoted by a controllable polar coordinate (r, θ) and O is the original point of the coordinate system. The radius of solid-line surface is $r_{b,2}$ (or $r'_{b,2}$) and of dashed-line surface is $r''_{b,2}$. (c) Comparing the varyings of three different two-atom blockade radius $r_{b,2}$ (dash-dotted magenta line), $r'_{b,2}$ (dashed blue line), $r''_{b,2}$ (dotted red line), and one antiblockade radius $r_{ab,2}$ (solid black line) as a function of Ω values, taking into account the vdWs RRI potential energy $V_{12}/\hbar = C_6/r_{12}^6$ for relatively low excited-state atoms with $C_6 \approx 2\pi \times 1\text{GHz } \mu\text{m}^6$ and the principal quantum number $n \sim 20 - 30$. The decay rate is set to be $\gamma = 2\pi \times 0.2\text{MHz}$. Inset: a detailed picture for $\Omega/2\pi \in [0, 0.1]$.

II. A TWO-ATOM SYSTEM

A. Two-atom blockade effect

Let us first recall the essence of a simple two-atom blockade scheme with the RRI $V_{12}(r_{12})$. See the caption of Fig. 1 for a detailed scheme description. When two atoms are in the double Rydberg state $|r_1 r_2\rangle$, they interact strongly due to the vdWs interaction, leading

to an interatomic distance-dependent energy shift by $V_{12}(r_{12}) = C_6/r_{12}^6$ [$\hbar = 1$ throughout the paper]. For the shifted energy that is larger than the laser excitation linewidth, the laser transition is out of resonance and only one of two atoms (e.g. atom 1) would be transferred to the Rydberg state at a time, resulting in very low doubly excited state population for Rydberg atoms. This is so-called *Rydberg blockade effect* [30].

To demonstrate the blockade efficiency quantitatively, a picture of *blockade sphere* with radius r_b is considered to be very useful. Within the sphere, only single-atom excitation is allowed if the mean interatomic distance is much smaller than r_b ; hence, we require a good definition of r_b . For two atoms confined in a sphere, there are two ways to define it:

(i) The easiest way to estimate $r_{b,2}$ (subscript 2 means the atomic number) relies on the model of a single laser-driven atom excited to Rydberg state with its linewidth dominated by the power broadening Ω [Ω is single-photon Rabi frequency for two-level atoms and effective two-photon Rabi frequency for three-level atoms], so that $r_{b,2}$ is defined as the interatomic distance at which the interaction energy equals the linewidth of excitation,

$$r_{b,2} = \left(\frac{C_6}{\sqrt{2}\Omega} \right)^{1/6}. \quad (1)$$

For a N -atom ensemble, a collective blockade radius is $r_{b,N} = (C_6/\sqrt{N}\Omega)^{1/6}$ [5].

(ii) Another generalized way uses the steady-state population $\langle \hat{\sigma}_{rr} \rangle$ of a single atomic Rydberg state under cw laser drivings that is $\langle \hat{\sigma}_{rr} \rangle = \Omega^2 / (2\Omega^2 + \gamma^2/4 + \Delta^2)$ to estimate its linewidth $w_1 = \sqrt{2\Omega^2 + \gamma^2/4}$ (clearly $w_1 \propto \sqrt{2}\Omega$) [31]. Therefore, the corresponding radius $r'_{b,2}$ takes the form of

$$r'_{b,2} = \left(\frac{2C_6}{\sqrt{8\Omega^2 + \gamma^2}} \right)^{1/6}. \quad (2)$$

So far, to our knowledge estimating blockade radius by the properties of single atom excitation has been the unique and robust way [26]. However, a full theoretical description of this laser-driven, strongly interacting multi-atom system is still challenging. On the purpose of improving the understandings for two-atom Rydberg blockade, we suggest a new definition for radius by directly solving the master equations of two interacting atoms [32]: $\partial_t \hat{\rho} = -i[\mathcal{H}, \hat{\rho}] + \mathcal{L}[\hat{\rho}]$, with the Hamiltonian \mathcal{H} describing the atom-field interaction as well as the vdWs interaction, the Lindblad operator $\mathcal{L}[\hat{\rho}]$ for the spontaneous decay process. Then the steady-state population $\langle \hat{\sigma}_{r_1 r_2} \rangle$ for double Rydberg state $|r_1 r_2\rangle$ is given by

$$\langle \hat{\sigma}_{r_1 r_2} \rangle = \frac{4\Omega^4}{(4\Omega^2 + \gamma^2/2 + 2\Delta^2)^2 + V_{12}^2 (V_{12} - 4\Delta) (4\Omega^2 + \gamma^2/4 + \Delta^2)}. \quad (3)$$

In the case of $\Delta = 0$, Eq. (3) reduces into $4\Omega^4 / \{(4\Omega^2 + \gamma^2/2)^2 + V_{12}^2 (4\Omega^2 + \gamma^2/4)\}$, showing a Lorentzian function of V_{12} with the two-atom excitation linewidth $w_2 = (4\Omega^2 + \gamma^2/2) / \sqrt{4\Omega^2 + \gamma^2/4}$ (clearly $w_2 \propto 2\Omega$). In a similar way, we are able to define a new blockade radius, as

$$r''_{b,2} \approx \sqrt[6]{\frac{C_6}{w_2}} = \left(\frac{C_6 \sqrt{16\Omega^2 + \gamma^2}}{8\Omega^2 + \gamma^2} \right)^{1/6}. \quad (4)$$

From the definitions of radius $r_{b,2}$, $r'_{b,2}$ and $r''_{b,2}$, we note $r''_{b,2} < r'_{b,2} \leq r_{b,2}$. In Fig. 1(c), we observe that they all show a slowly decreasing as Ω increases and $r''_{b,2}$ persists slightly smaller than $r_{b,2}$ and $r'_{b,2}$. $r_{b,2}$ and $r'_{b,2}$ have a perfect overlap if $\Omega \gg \gamma$ except for very small Ω values [see the inset of Fig. 1(c)]. By then, the blockade efficiency can be roughly quantified by the radius, i.e. a strong blockade regime is defined by the two-atom distance r_{12} being significantly smaller than the blockade radius. For a large Ω , the blockade effect is weaker.

According to the results of most experiments e.g. Ref. [5], they need the mean interaction distance being smaller than the blockade radius by several orders of magnitude i.e. $V_{12} \gg \Omega$ for the study of strong blockade effect, so that such differences between $r_{b,2}$, $r'_{b,2}$ and $r''_{b,2}$ may be negligible; however, when working in the partial blockade regime where $V_{12} \approx \Omega$, they may become important for the results, owing to its sensitive dependence of double excitation probability on the interatomic distance as well as Rabi frequency [25]. In the present work, we use $r''_{b,2}$ to represent the two-atom blockade radius.

B. Two-atom antiblockade effect

Equation (3) also provides us a new route to investigate the antiblockade efficiency. As first predicted by C. Ates *et al.* [33] and later experimentally verified by T. Amthor *et al.* [34], the antiblockade effect is a specific effect with high doubly excited state population in the blockade regime when the laser detuning matches the Rydberg-Rydberg interaction energy. It can emerge for instance if the RRI energy shift equals the two-photon detuning based on the Autler-Townes splitting mechanism in an atomic three-level system. According to the concept of antiblockade, the two-atom antiblockade condition can be written as $2\Delta = V_{12}(r)$, leading to the steady-state population $\langle \hat{\sigma}_{r_1 r_2} \rangle$

$$\langle \hat{\sigma}_{r_1 r_2} \rangle = \frac{4\Omega^4}{(4\Omega^2 + \gamma^2/2)^2 + V_{12}^2 \gamma^2/4}, \quad (5)$$

where the antiblockade radius $r_{ab,2}$ is

$$r_{ab,2} = \left(\frac{\gamma C_6}{8\Omega^2 + \gamma^2} \right)^{1/6}. \quad (6)$$

As shown in Fig. 1(c), compared with the blockade radius, the antiblockade radius $r_{ab,2}$ (denoted by solid black line) is small than $r''_{b,2}$ and has the same tendency as the blockade radius for Ω changes.

Finally, we conclude that inside the blockade sphere, once the antiblockade condition is met, the probability for double Rydberg excitation will be strikingly enhanced; beyond the sphere regime, the role of RRI is poor which makes the blockade mechanism invalid, so both high single-atom and multi-atom excitation probabilities are possible. To observe obvious two-atom antiblockade behavior, we suggest the interatomic distance $r_{ab,2} < r_{12} < r''_{b,2}$ as well as the condition $2\Delta - V_{12}(r) = 0$ is met.

III. A THREE-ATOM SYSTEM

A. Deformed blockade sphere

The *blockade sphere* picture is identified to be robust when demonstrating the two-atom blockade experiments [12, 13], which has extended to a N -atom ensemble with one excited atom, so-called "superatom" [35]. On the other hand, while increasing the real number of atoms from two to three, the three-atom excitation dynamics would show an unexpected and qualitative change. This idea was considered in an isosceles triangle configuration [29] near Förster resonance interactions [36].

In the present section, our goal is to develop a generalized model of a three-atom system in a 2D space, for the purpose of studying spatially anisotropic deformation of blockade sphere due to the presence of atom 3. The assumption of a spherical-type blockade surface is widely accepted, which gives rise to a clear picture for Rydberg studies. We show that this assumption is exactly correct only if the separation r_{12} is much smaller than the blockade radius, otherwise, the blockade surface is no longer a spherical shape.

Our model is depicted in Fig. 1(b). Atoms 1 and 2 are initially prepared on x axis with a fixed distance r_{12} and its central point O describing the original point of coordinate system. In the same space, there exists atom 3 whose position is defined as (r, θ) with r the distance from O point and θ the directional angle with respect to $+x$ axis. Then the interatomic separations r_{13} (atom 1 and atom 3) and r_{23} (atom 2 and atom 3) can be expressed as:

$$r_{13(23)} = \sqrt{(x_3 \pm r_{12}/2)^2 + y_3^2} \quad (7)$$

where $(x_3, y_3) = (r/\sqrt{1 + \tan^2 \theta}, r \tan \theta / \sqrt{1 + \tan^2 \theta})$. Differing from a two-atom system where only interaction

V_{12} plays roles, such a three-atom scheme offers a feasible platform to study both interactions and quantum interference from three different energy channels V_{12} , V_{13} and V_{23} . In Ref. [29], authors consider one type of configuration: an isosceles triangle. When the third atom is brought closer to the atomic pair, by tuning the laser pulse duration and laser amplitude, a significant increase for the double Rydberg excitation is observed. The reason for this increase we think essentially comes from the shrunken of blockade surface due to the multi-channel quantum interference.

In our numerical explorations, for relative low Rydberg levels (e.g. $n \sim 20 - 30$), the vdW coefficient is $C_6 = 2\pi \times 1000 \text{ MHz } \mu\text{m}^6$ [37], which for $\Omega/2\pi = 1.0 \text{ MHz}$ and $\gamma/2\pi = 0.2 \text{ MHz}$ gives the blockade radius $r''_{b,2} = 2.8155 \mu\text{m}$. We note that this value is even smaller than the collective blockade radius for three atoms based on the former definition $[r_{b,3} = (C_6/\sqrt{3}\Omega)^{1/6} \approx 2.8856 \mu\text{m}]$. Besides, to perform the calculations more efficiently, we make two assumptions: (i) If atom 3 is placed too close to atoms 1 or 2, the interaction V_{13} (V_{23}) $\rightarrow +\infty$; in this case, we treat it as a two-atom problem where the critical distance for r_{13} (r_{23}) is chosen as $r_c = 1 \mu\text{m}$ ($1 \mu\text{m}$ is the characteristic wavelength of light needed for internal-state manipulation [12]). (ii) By directly solving the three-atom master equations $\partial_t \hat{\rho} = -i[\mathcal{H}, \hat{\rho}] + \mathcal{L}[\hat{\rho}]$, we define a new quantity $P_2(r, \theta) = |grr\rangle \langle grr| + |rgr\rangle \langle rgr| + |rrg\rangle \langle rrg|$ to describe the probability of simultaneously exciting any two of three atoms to Rydberg states. In a polar coordinate system, the three-atom blockade radius $r_{b,3}$ is numerically determined by $P_2(r_{b,3}, \theta) = 0.5(P_2(+\infty, \theta) - P_2(0, \theta))$. When separation $r \rightarrow +\infty$, P_2 attains its maximum for non-blockade regimes and when $r \rightarrow 0$, P_2 is minimal for strong blockade regimes.

In Fig. 2(a), the red arrow points to the direction of an increasing two-atom distance r_{12} along which the steady-state population $\langle \hat{\sigma}_{r_1 r_2} \rangle$ undergoes a continuous transition from low excitations ($\langle \hat{\sigma}_{r_1 r_2} \rangle \approx 0$, black) to the saturated excitations of two-level atoms ($\langle \hat{\sigma}_{r_1 r_2} \rangle \approx 0.25$, white). The green circle denotes the two-atom blockade surface. Fig. 2(b)-(d) are graphed in the 2D polar coordinate (r, θ) of atom 3. When atom 3 presents, the original two-atom blockade sphere (solid green circle) reveals different strengths of deformations, which strongly depend on the two-atom distance r_{12} [see dashed white circles]. From (b) to (d) by respectively choosing $r_{12} = 1 \mu\text{m}$, $2 \mu\text{m}$ and $3 \mu\text{m}$, we find the three-atom blockade spheres turn to be radius-reducing long elliptical shape. The clear shrunken property of the sphere surface makes the blockade effect more difficult in a three-atom ensemble than in a two-atom one. We also find the two-atom distance r_{12} has a significant role in the three-atom blockade. Compared to $r''_{b,2}$, the smaller r_{12} is, the less broken or deformed of blockade surface is observed while adding the third atom. Because in this case, interactions V_{13} and V_{23} are always smaller or comparable with V_{12} [see Fig. 2(b)]. By contrast, when r_{12} is close to $r''_{b,2}$, three different interaction channels result in strong quantum interference

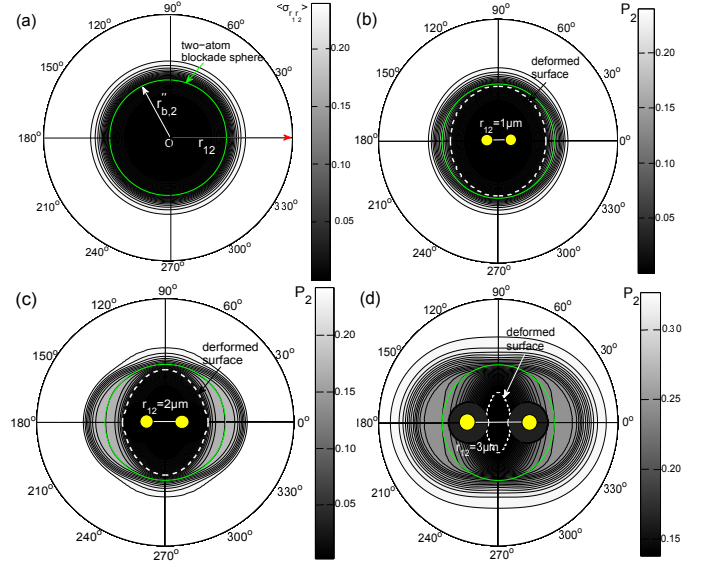


FIG. 2: (Color online) The two-atom blockade sphere is denoted by a solid green circle with radius $r''_{b,2}$. (a) Along the direction of red arrow, the two-atom distance r_{12} increases as the steady-state population $\langle \sigma_{r_1 r_2} \rangle$ attaining 0.25 (white) from 0 (black). (b)-(d) Deformed three-atom blockade sphere surface (dashed white curve) for $r_{12} = 1 \mu\text{m}$, $2 \mu\text{m}$ and $3 \mu\text{m}$, respectively. Two yellow circles denote atoms 1 and 2. The double excitation probability P_2 is shown by the gray-level diagram from 0 (black) to 0.25 (white) in (b) and (c), and from 0.15 (black) to 0.35 (white) in (d). $\Delta = 0$ and other parameters are defined in the text.

effect, yielding a strong deformed surface [see Fig. 2(d)].

Based on our numerical results, it is interesting to find the deformation effect in a three-atom system shows spatially anisotropic properties that the deformed surface becomes a long ellipse rather than a circle or an oblate ellipse. To demonstrate this finding, we consider two extreme cases: (i) a 1D chain of atoms with $\theta = 0$, (ii) an isosceles triangle with $\theta = \pi/2$. In case (i), when atom 3 is closing to the atomic pair from $+x$ axis, $r_{13}^{(i)} = r + r_{12}/2$, $r_{23}^{(i)} = |r - r_{12}/2|$; in case (ii), when atom 3 is coming from $+y$ axis, $r_{13}^{(ii)} = r_{23}^{(ii)} = \sqrt{r_{12}^2/4 + r^2}$. For given r_{12} and r , we note that $r_{23}^{(i)} < r_{13}^{(ii)} < r_{13}^{(i)}$. A complete asymmetric excitation property for a chain model creates a larger deformation strength than for a symmetric isosceles triangular model; so that if r_{12} is small $r_{13}^{(i)} \approx r_{23}^{(i)}$, a long elliptical-shape surface is not so clear compared with a large r_{12} case.

Another interesting result is for two-atom distance $r_{12} (= 3 \mu\text{m})$ that is comparable with $r''_{b,2}$, as shown in Fig. 2(d), the double Rydberg excitation probability P_2 can not be absolutely suppressed even if $r \rightarrow 0$. At the same time, at $r \rightarrow +\infty$, P_2 approaches 0.35 which is larger than the saturation limit ($\langle \sigma_{r_1 r_2} \rangle_{\text{max}} = 0.25$) for two-level atomic systems. We think this is a regime for partial blockade behavior (i.e. imperfect blockade) which

usually appears at the boundary of the region of finite size [21].

B. Antiblockade for multi-atom systems: take three atoms as an example

In section II.B, we study the two-atom antiblockade and obtain a quantified antiblockade radius $r_{ab,2}$ for optimizing its efficiency. That is the interatomic distance r_{12} should be $r_{ab,2} < r_{12} < r''_{b,2}$, beyond this regime, if $r_{12} < r_{ab,2}$, the antiblockade is inefficient; otherwise if $r_{12} > r''_{b,2}$, both single and double Rydberg states will be populated. In this section, we take a three-atom system as an example to explore a generalized antiblockade condition form for multi-atom systems.

In a three-atom system, we predict the antiblockade condition to be $2\Delta - V(r) = 0$ [38] with $V(r)$ the RRI between any two atoms $V_{12}(r_{12})$, $V_{13}(r_{13})$ and $V_{23}(r_{23})$. First, we assume r_{12} is fixed as well as $V_{12}(r_{12}) \neq 2\Delta$, so that by changing the position of atom 3, it is possible to meet two resonant conditions: $V_{13}(r_{13}) = 2\Delta$ and $V_{23}(r_{23}) = 2\Delta$ for a given detuning Δ .

In Fig. 3(a), for a given detuning ($\Delta = 10\text{MHz}$) and two-atom distance ($r_{12} = 2\mu\text{m}$), we show the antiblockade trajectory as two circles (blue and red) whose centers locate at atom 1 and atom 2 and radius is $r_{13} = r_{23} \approx 2.6\mu\text{m}$, respectively to meet the resonant conditions of $V_{13}(r_{13}) = 2\Delta$ and $V_{23}(r_{23}) = 2\Delta$. We select five points on two trajectories and plot their excitation probabilities P_2 as a function of distance r in Fig. 3(b), corresponding to three different angles $\theta = \pi/2$ (A, solid blue), $\pi/3$ (B and C, dashed red), $\pi/6$ (D and E, dotted black). The x -axis-labeling r denotes the distance from original point O (not from atoms). From Fig. 2(c), we note that points A, B, D are within the regime of deformed blockade sphere that render the excitation probability $P_2 \leq 0.25$. However, for points C and E, P_2 exceeds 0.25 due to the imperfect antiblockade near the boundary of blockade surface. In addition, we also find that except for $\theta = \pi/2$ and $3\pi/2$ that is a symmetric triangular structure (e.g. point A), for other angles θ there exist two distinguishable antiblockade resonances, locating at

$$r = \sqrt{\left(\frac{C_6}{2\Delta}\right)^{1/3} - \frac{r_{12}^2 \tan^2 \theta}{4(1 + \tan^2 \theta)}} \pm \frac{r_{12}}{2\sqrt{1 + \tan^2 \theta}} \quad (8)$$

Second, we introduce another picture to study the antiblockade excitation properties. Figure 3(c) shows the double excitation probability P_2 by varying detuning Δ . We set separations $r_{12} = 2\mu\text{m}$, $r = 2\mu\text{m}$, and $\theta = \pi/2$, $\pi/3$ and $\pi/6$ for three triangular configurations. Except for $\theta = \pi/2$ that $r_{13} = r_{23}$ giving rise to two resonant excitations (denoted by solid blue lines), at $\theta = \pi/3$ and $\pi/6$, we observe three different resonant peaks for P_2 at $\Delta_1 = C_6/2r_{12}^6$ (fixed, $\Delta_1 \approx 49.1\text{MHz}$), $\Delta_2 = C_6/2r_{13}^6$ and $\Delta_3 = C_6/2r_{23}^6$ whose amplitudes $P_2(\Delta)$ rely on the distance r . A small r value for large positive detunings

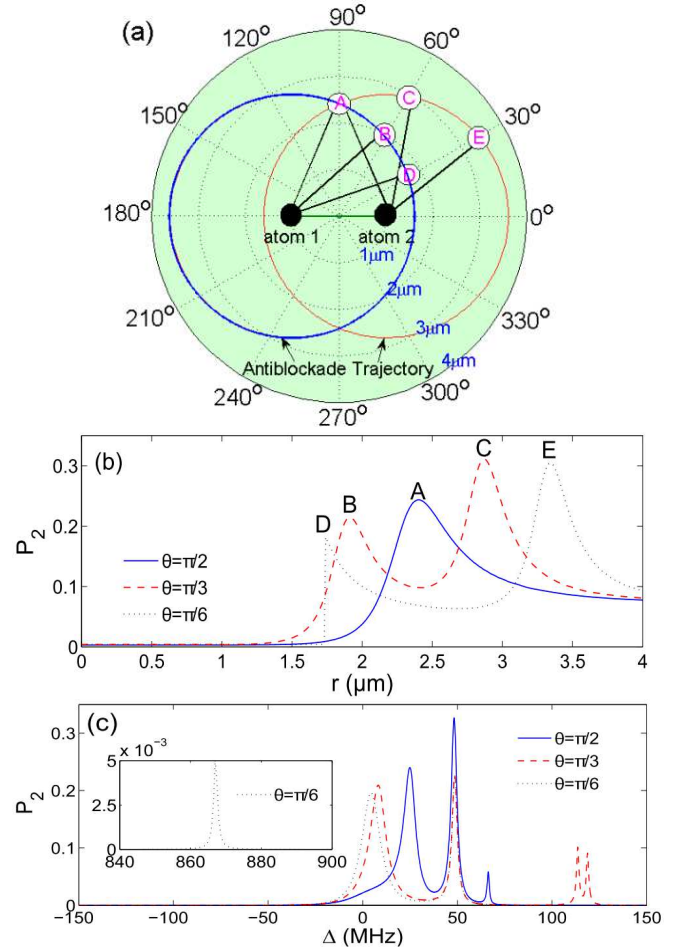


FIG. 3: (Color online) (a) Schematic of Rydberg antiblockade trajectory. Two crossed circles correspond to two antiblockade conditions: $V_{13}(r_{13}) = 2\Delta$ (left blue circle) and $V_{23}(r_{23}) = 2\Delta$ (right red circle). The corresponding double Rydberg-state excitation probabilities P_2 as varied distances at the points of A-E are plotted in (b). Parameters are $\Delta = 10\text{MHz}$, $r_{12} = 2\mu\text{m}$, and others are the same as in Fig. 2. (c) Probabilities P_2 vs the detuning Δ for different directional angles $\theta = \pi/2$ (solid blue), $\pi/3$ (dashed red) and $\pi/6$ (dotted black).

inside the regime of antiblockade radius results in a poor antiblockade efficiency [see $P_2(\Delta_3)$ at $\theta = \pi/3$ and $\pi/6$]. This finding agrees well with the two-atom case. While, at the side of negative detuning or zero detuning values, $P_2(\Delta)$ is mostly suppressed, which strongly verifies that the generalized antiblockade condition $2\Delta = V(r)$ is correct.

IV. CONCLUSIONS

In summary, we thoroughly study the Rydberg blockade and antiblockade effects in two- and three-atom systems. Starting from a typical two-atom blockade sphere model, we quantify the two-atom blockade and antiblock-

ade efficiency by introducing more rigorous definitions for the radius, based on theoretically solving the two-interacting-atom master equations. When turning to the three-atom case, we observe that the spherical surface would occur strong spatial anisotropic deformation with a reduced radius which is sensitive related to the mean interatomic distance. This fact renders the blockade effect more difficult to achieve in a three-atom system than in a two-atom one. The anisotropy property stems from the asymmetric Rydberg-Rydberg interactions for atoms 1, 3 and atoms 2, 3. In addition, we also numerically investigate a generalized antiblockade condition in a three-atom system and show the double Rydberg excitation properties are importantly affected by the blockade and antiblockade boundaries.

On the one hand, our results are consistent with a collective blockade radius $r_{b,N} \approx (C_6/\sqrt{N}\Omega)^{1/6}$ for a superatom scheme which implies that $r_{b,N}$ will reduce if

we increase the atomic number N ; on the other hand, the idea that the deformation of blockade sphere is spatially anisotropic is brightly new and may stimulate new explorations for Rydberg experiments in various 2D optical lattices in the future.

This work is supported by the National Basic Research Program of China (973 Program) under Grant No. 2011CB921604, the National Natural Science Foundation of China under Grants Nos. 11104076, 11004057, 11234003 and 11374003, the Specialized Research Fund for the Doctoral Program of Higher Education No. 20110076120004, the Young Scholar of Henan normal university No. 0102640065, the 'Chen Guang' project supported by Shanghai Municipal Education Commission and Shanghai Education Development Foundation under grant No. 10CG24, the Shanghai Rising-Star Program under grant No. 12QA1401000, and the Fundamental Research Funds for the Central Universities.

-
- [1] A. Glaetzle, R. Nath, B. Zhao, G. Pupillo and P. Zoller, Phys. Rev. A **86** 043403(2012).
 - [2] H. Weimer, R. Löw, T. Pfau and H. Büchler, Phys. Rev. Letts. **101** 250601 (2008).
 - [3] T. Pohl, E. Demler and M. Lukin, Phys. Rev. Letts. **104** 043002 (2010).
 - [4] F. Mauher, N. Henkel, M. Saffman, W. Królikowski, S. Skupin and T. Pohl, Phys. Rev. Letts. **106** 170401 (2011).
 - [5] R. Heidemann, U. Raitzsch, V. Bendkowsky, B. Butscher, R. Löw, L. Santos and T. Pfau, Phys. Rev. Letts. **99** 163601 (2007).
 - [6] J. Honer, R. Löw, H. Weimer, T. Pfau and H. Büchler, Phys. Rev. Letts. **107** 093601 (2011).
 - [7] D. Jaksch, J. I. Cirac, P. Zoller, S. L. Rolston, R. Côté and M. D. Lukin, Phys. Rev. Letts. **85** 2208 (2000).
 - [8] M. D. Lukin, M. Fleischhauer, R. Côté, L. M. Duan, D. Jaksch, J. I. Cirac, and P. Zoller, Phys. Rev. Letts. **87** 037901 (2001).
 - [9] K. Singer, M. R-Lamour, T. Amthor, L. Marcassa and M. Weidemüller, Phys. Rev. Letts. **93** 163001 (2004).
 - [10] Y. O. Dudin and A. Kuzmich, Science **336** 887 (2012); P. Grangier, Science **336** 812 (2012).
 - [11] P. Schauss, M. Cheneau, M. Endres, T. Fukuhara, S. Hild, A. Omran, T. Pohl, C. Gross, S. Kuhr and I. Bloch, Nature **491** 87 (2012).
 - [12] E. Urban, T. A. Johnson, T. Henage, L. Isenhower, D. D. Yavuz, T. G. Walker and M. Saffman, Nat. Phys. **5** 110 (2009).
 - [13] A. Gaetan, Y. Miroshnychenko, T. Wilk, A. Chotia, M. Viteau, D. Comparat, P. Pillet, A. Browaeys and P. Grangier, Nat. Phys. **5** 115 (2009).
 - [14] H. Kübler, J. Shaffer, T. Baluktsian, R. Löw and T. Pfau, Nature Phot. **4** 112 (2010).
 - [15] M. Müller, A. Kölle, R. Löw, T. Pfau, T. Calarco and S. Montangero, Phys. Rev. A **87** 053412 (2013).
 - [16] M. Saffman, T. Walker and K. Molmer, Rev. Mod. Phys. **82** 2313 (2010) and references therein.
 - [17] H. Weimer, M. Müller, I. Lesanovsky, P. Zoller and H. Büchler, Nat. Phys. **6** 382 (2010).
 - [18] M. R-Lamour, T. Amthor, J. Deiglmayr and M. Weidemüller, Phys. Rev. Letts. **100** 253001 (2008).
 - [19] T. Johnson, E. Urban, T. Henage, L. Isenhower, D. Yavuz, T. Walker and M. Saffman, Phys. Rev. Letts. **100** 113003 (2008).
 - [20] M. Viteau, M. Bason, J. Radogostowicz, N. Malossi, D. Ciampini, O. Morsch and E. Arimondo, Phys. Rev. Letts. **107** 060402 (2011).
 - [21] D. Petrosyan, M. Hönig and M. Fleischhauer, Phys. Rev. A **87** 053414 (2013).
 - [22] U. Raitzsch, V. Bendkowsky, R. Heidemann, B. Butscher, R. Löw and T. Pfau, Phys. Rev. Letts. **100** 013002 (2008).
 - [23] M. Viteau, P. Huillery, M. Bason, N. Malossi, D. Ciampini, O. Morsch, E. Arimondo, D. Comparat and P. Pillet, Phys. Rev. Letts. **109** 053002 (2012).
 - [24] M. R-Vincent, C. Hofmann, H. Schempp, G. Günter, S. Whitlock and M. Weidemüller, Phys. Rev. Letts. **110** 045004 (2013).
 - [25] L. Béguin, A. Vernier, R. Chicireanu, T. Lahaye and A. Browaeys, Phys. Rev. Letts. **110** 263201 (2013); M. Weidemüller, Physics **6** 71 (2013).
 - [26] D. Tong, S. Farooqi, J. Stanojevic, S. Krishnan, Y. Zhang, R. Cote, E. Eyler and P. Gould, Phys. Rev. Letts. **93** 063001 (2004).
 - [27] J. Pritchard, D. Maxwell, A. Gauguier, K. Weatherill, M. Jones and C. Adams, Phys. Rev. Letts. **105** 193601 (2010).
 - [28] J. Pritchard, C. Adams and K. Molmer, Phys. Rev. Letts. **108** 043601 (2012).
 - [29] T. Pohl and P. Berman, Phys. Rev. Letts. **102** 013004 (2009).
 - [30] D. Comparat and P. Pillet, J. Opt. Soc. Am. B **27** A208 (2010), and reference therein.
 - [31] M. Hönig, D. Muth, D. Petrosyan and M. Fleischhauer, Phys. Rev. A **87** 023401 (2013).
 - [32] J. Qian, L. Zhou and W. Zhang, Phys. Rev. A **87** 063421 (2013).
 - [33] C. Ates, T. Pohl, T. Pattard and J. M. Rost, Phys. Rev. Letts. **98** 023002 (2007).

- [34] T. Amthor, C. Giese, C. Hofmann and M. Weidemüller, Phys. Rev. Letts. **104** 013001 (2010).
- [35] V. Vuletic, Nature Phys. **2** 801 (2006).
- [36] I. Ryabtsev, D. Tretyakov, I. Beterov, V. Entin and E. Yakshina, Phys. Rev. A **82** 053409 (2010).
- [37] K. Singer, J. Stanojevic, M. Weidemüller and R. Côté, J. Phys. B: At. Mol. Opt. Phys. **38** S295 (2005).
- [38] W. Li, C. Ates and I. Lesanovsky, Phys. Rev. Letts. **110** 213005 (2013).